Transverse Fluctuations Control the Assembly of Semiflexible Filaments

Valerio Sorichetti[1,2] and Martin Lenz[2,3]
[1]Institute of Science and Technology Austria, 3400 Klosterneuburg, Austria
[2]Laboratoire de Physique Théorique et Modèles Statistiques (LPTMS), CNRS, Université Paris-Saclay, F-91405 Orsay, France
[3]PMMH, CNRS, ESPCI Paris, PSL University, Sorbonne Université, Université de Paris, F-75005 Paris, France

(Received 6 March 2023; accepted 24 October 2023; published 27 November 2023)

The kinetics of the assembly of semiflexible filaments through end-to-end annealing is key to the structure of the cytoskeleton, but is not understood. We analyze this problem through scaling theory and simulations, and uncover a regime where filaments' ends find each other through bending fluctuations without the need for the whole filament to diffuse. This results in a very substantial speedup of assembly in physiological regimes, and could help with understanding the dynamics of actin and intermediate filaments in biological processes such as wound healing and cell division.

DOI: 10.1103/PhysRevLett.131.228401

The self-assembly of cytoskeletal filaments is crucial for many cellular functions, including wound healing [1] and cell division [2]. The growth kinetics of these filaments strongly influences the morphology of the networks they form, from bundled to entangled structures [3–7]. Unlike the well-understood actin filaments and microtubules [8], intermediate filaments of vimentin and keratin crucial for cell shape and mechanical integrity [9] mainly grow by end-to-end annealing [10–14]. This mechanism is also at work in wormlike micelles [15], DNA [16], and some synthetic polymers [17], and plays a secondary role in the assembly of actin [18,19] and microtubules [20]. As filaments elongate by end-to-end annealing, their diffusion becomes slower due to an increased viscous drag. The time needed to find other reaction partners then increases, giving rise to *diffusion-limited* growth [21]. Theoretical models have been proposed to describe the dependence of the polymer growth kinetics on physical properties such as length, flexibility, and concentration [22–28]. Many have, however, employed the Gaussian chain model, which provides a poor description of cytoskeletal filaments [8].

Here, we instead tackle the more general case of semiflexible filaments, and uncover a new assembly regime driven by transverse fluctuations. While rigid rods react slowly due to the need of mobilizing the center of mass [Fig. 1(a)], these fluctuations speed up the search of bonding partners, leading to faster assembly [Fig. 1(b)]. We first describe the growth regimes successively encountered by a growing filament, then validate the resulting scaling laws using Brownian dynamics simulations.

We model the annealing of semiflexible filaments as an irreversible reaction whereby an i mer and a j mer form an $i+j$ mer (Fig. 1). The reaction rate constant $K_{i,j}$ generically depends on the lengths of the reacting filaments [21]. Filaments undergo annealing *via* reactive sites (monomers) located at their ends that bind immediately upon contact, and we assume the system is dilute enough to ignore steric constraints, e.g., entanglements [29,30]. We also neglect hydrodynamic interactions, and describe filament dynamics with the Rouse model [29]. Finally, our scaling discussion ignores numerical prefactors as well as length polydispersity, and thus considers a single typical contour length L and reaction rate constant $K(L)$.

The annealing rate of a collection of filaments of length L stems from the dynamics of their reaction sites [22–27]. To describe it, we assume a scaling form $x(t) \propto t^{\alpha}$ for the root-mean-square displacement of one such site. For normal diffusion, $\alpha = 1/2$, while $\alpha = 1/4$ at short times in a long Gaussian polymer [29]. If $\alpha > 1/d$, with d the dimension of space, the monomer explores space in a *noncompact* manner. This means that, if we approximate this exploration as a discrete process in which a site of volume b^d (with b the monomer size) is visited at each step, the number of sites visited at time t is much smaller than $[x(t)/b]^d$. We assume that the reactants are uniformly distributed before the reaction and that the reaction takes

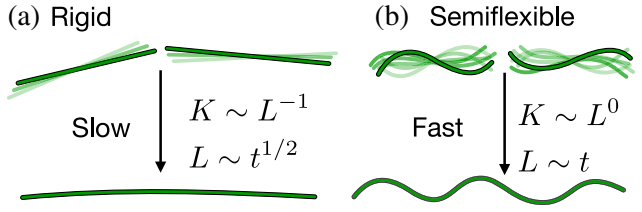

FIG. 1. Rigid filaments (a) assemble by displacing their center of mass, which results in a reaction rate $K \propto L^{-1}$, with L the mean contour length, and slow growth ($L \propto t^{1/2}$). Here, we show that semiflexible filaments (b) take advantage of transverse fluctuations to quickly join their ends, resulting in a constant reaction rate ($K \propto L^{0}$) and faster growth ($L \propto t$).

place immediately when the reactants come within a distance $\approx b$. Then, in $d = 3$ [26]

$$K^{-1} \approx \int_{\tau_b}^{\infty} x^{-3}(t)\mathrm{d}t, \tag{1}$$

where τ_b is the time a monomer takes to move over a distance b. In the regimes considered below, this results in $K(L) \propto L^{-\lambda}$, where the exponent $\lambda \geq 0$ depends on the physical process underlying the motion of the reactive sites. The number density of filaments ν evolves as $\dot{\nu} = -K(L)\nu^2$. Since $\nu = cb/L$, with c the total monomer density, this implies $L(t) \propto t^{1/(1+\lambda)}$ [31–33].

Starting from a solution of monomers, filaments are initially much shorter than the persistence length L_p [34], and thus behave as rigid rods ($L_p = \infty$). Their ends undergo diffusive dynamics, i.e., $x^2(t) \approx Dt$ where D is the center-of-mass diffusion coefficient of the filament. If each monomer is subjected to a viscous friction ζ, we have $D = k_B T b/\zeta L$ [29]. Equation (1) with $\tau_b \approx b^2/D$ thus yields $K \approx b^3\tau_b^{-1} \approx k_B T b^2/\zeta L \approx b^3\tau^{-1}(b/L)$, where $\tau \approx b^2\zeta/k_B T$ is the time a free monomer takes to move by b. Since $L(t) \propto t^{1/(1+\lambda)}$, the filament length reads

$$L(t)/b \approx (cb^3 t/\tau)^{1/2}. \tag{2}$$

Thus, both center-of-mass diffusion and filament growth slow down over time.

As the filaments elongate, bending fluctuations become relevant even as $L \ll L_p$. Indeed, the short-time dynamics of the reactive sites then becomes dominated by bending modes. Their root-mean-square displacement thus grows with time predominantly in the direction perpendicular to the local filament contour [34–38]. This results in a short-time subdiffusive regime, $x(t) \propto t^{3/8}$. This lasts until the time $\tau_f \approx \tau(L^4/L_p b^3)$ required to relax the longest-wavelength bending mode of the filament. Subsequently, center-of-mass diffusion dominates filament motion. The typical monomer displacement thus reads

$$x(t) \approx \begin{cases} (b^9/L_p)^{1/8}(t/\tau)^{3/8} & \tau \lesssim t \lesssim \tau_f \\ (b^3/L)^{1/2}(t/\tau)^{1/2} & t \gtrsim \tau_f. \end{cases} \tag{3}$$

In the regime considered here, the monomer displacement time τ_b is computed from the short-time regime of Eq. (3), yielding $\tau_b \approx \tau(L_p/b)^{1/3}$. If the total duration τ_f of the bending-fluctuations-dominated regime is much longer than the monomer displacement time τ_b, this regime dominates the integral of Eq. (1), and therefore the reaction rate. We may equivalently require $L \gg L^* \approx b(L_p/b)^{1/3}$. Since $L(t) \propto t^{1/(1+\lambda)}$, this yields

$$K \approx b^3\tau_b^{-1} \approx b^3\tau^{-1}(L_p/b)^{-1/3} \quad (\text{for } L \gg L^*). \tag{4}$$

Thus, for filaments longer than L^*, the reaction rate is *independent* of L, as also found for first-passage problems involving semiflexible filaments [39,40]. A scaling argument leading directly to Eq. (4) is presented in the Supplemental Material [41]. As illustrated in Fig. 1(b), transverse fluctuations then allow the reactive sites to "find" each other without center-of-mass motion. As the filaments elongate, their center-of-mass motion slows down, but the short-time dynamics of the reaction sites remains the same. This accounts for the independence of K on L and implies a constant growth speed:

$$L(t)/b \approx cb^3 t/\tau_b. \tag{5}$$

Mathematically, this stems from the $\tau_b \lesssim t \lesssim \tau_f$ time domain dominating the integral of Eq. (1) when $L \gg L^*$. Equation (5) is valid for $L \gg L^*$, while shorter filaments behave as rigid rods [Eq. (2)]. At the crossover between these two regimes, filaments have a length $L^* \ll L_p$, meaning that bending fluctuations overtake center-of-mass diffusion before the filaments become fully flexible. The crossover time reads $t^* = \tau(cb^3)^{-1}(L_p/b)^{2/3}$.

As the filaments eventually grow much longer than the persistence length ($L \gg L_p$), the short-time dynamics of the reactive sites is still dominated by the bending modes and independent of L [Eq. (3)]. At the time $\tilde{\tau}_f = \tau(L_p/b)^3$, the monomer displacement $x(t)$ becomes of order L_p. For later times, the filament behaves as a Gaussian chain [37,38] governed by Rouse relaxation modes [29]. Segments of the filaments with length $\approx L_p$ then diffuse while elastically coupled with the neighboring segments, leading to a slow, subdiffusive regime $x(t) \propto t^{1/4}$. This lasts up to the Rouse relaxation time $\tau_R = \tau(L_p L^2/b^3)$. Subsequently, the segments of the chain essentially move together and their displacement is again dominated by center-of-mass diffusion. Combining these three regimes (bending fluctuations, Rouse modes, and center-of-mass diffusion), we write the following for $L \gg L_p$:

$$x(t) \approx \begin{cases} (b^9/L_p)^{1/8}(t/\tau)^{3/8} & \tau \lesssim t \lesssim \tilde{\tau}_f \\ L_p(t/\tilde{\tau}_f)^{1/4} & \tilde{\tau}_f \lesssim t \lesssim \tau_R \\ (Dt)^{1/2} & t \gtrsim \tau_R, \end{cases} \tag{6}$$

where $D(L)$ is the diffusion constant of the "rigid rod" regime. The integral in Eq. (1) can now be split into three pieces, the last ($t \gtrsim \tau_R$) of which is negligible, yielding

$$K^{-1} \approx \tau b^{-3}(L_p/b)^{1/3}\left[1 + (3/4)(L/L^{**})^{1/2}\right], \tag{7}$$

where $L^{**} = L_p(L_p/b)^{2/3}$ and where each term of the sum stems from one of the remaining pieces of the integral. When $L \gg L^{**}$, the reaction rate thus crosses over from the bending-fluctuations-dominated regime of Eq. (4) to a

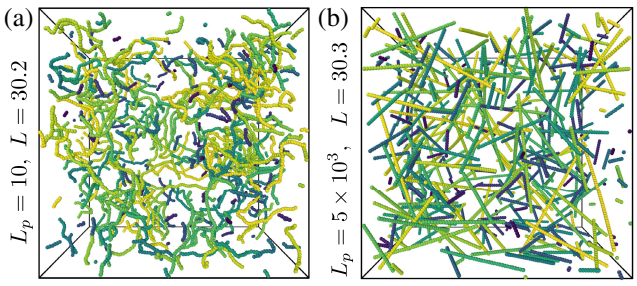

FIG. 2. Simulation snapshots ($N = 8000$ beads) of systems with the same mean contour length L and concentration ($c = 10^{-2}$) but with different persistence lengths L_p putting them in the fluctuations-driven (a) and rigid-rod-like (b) regimes. Shorter filaments are colored darker than longer ones.

Gaussian regime with $K \approx b^3\tau^{-1}(L/L_p)^{-1/2}$. In this regime, the mean contour length increases as

$$L(t)/L^* \approx (cb^3t/\tau)^{2/3}. \tag{8}$$

The crossover time associated with L^{**} is $t^{**} = \tau(cb^3)^{-1}(L_p/b)^2$. This last regime can be understood as follows: after the transverse fluctuations have relaxed ($t > \tilde{\tau}_f$), the monomers perform a *compact exploration* of space (i.e., their trajectories densely fill space) and quickly explore the region of size $R \approx L^{1/2}$ occupied by the filaments. The filaments then behave as diffusing reactive spheres with radius $R \propto L^{1/2}$ and diffusion coefficient $D \propto L^{-1}$. Their reaction rate then obeys the well-known Smoluchowski formula [47], $K = 4\pi DR \propto L^{-1/2}$, which results in $L \propto t^{2/3}$ [26]. Equation (8) is valid up to $L = L_p^3/b^2$, after which the filament starts to feel its own excluded volume and its dynamics changes [38].

Our scaling results rest on two main assumptions: that the system is characterized by a single typical contour length L and reaction rate constant $K(L)$, and that steric effects can be neglected. To test the robustness of our predictions when these assumptions are relaxed, we run Brownian dynamics simulations of semiflexible polymers undergoing irreversible end-to-end annealing. The polymers are purely repulsive Lennard-Jones beads of diameter $\sigma = 1$ connected by finite-extensible nonlinear elastic springs [48]. The Lennard-Jones interaction energy is $\epsilon = 1$. The system size is $N = 8000$ monomers, but we also simulated smaller systems ($N = 1000$, 4096) to check that there are no significant finite-size effects (Supplemental Material). To simulate semiflexible filaments, we impose an angular potential [49] $U_{\text{ang}}(\theta) = \varepsilon_b[1 - \cos(\theta)]$ to bonded triplets, where θ is the triplet angle and ε_b the bending stiffness. For stiff enough filaments $L_p = \varepsilon_b/k_BT$, which we validate by analyzing the bond orientation correlation function (Supplemental Material) and use throughout. We consider L_p values ranging between 10 [Fig. 2(a)] and 5×10^3 [Fig. 2(b)] (filaments with $L_p < 10$ tend to form spurious loops [50]). To test the validity of our predictions as the concentration c is increased from the dilute to the concentrated regime, we consider $c = 10^{-3}$, 10^{-2}, and 10^{-1}. We note that these values encompass typical ones found for vimentin intermediate filaments in living cells, which are between 0.1 and 1 mg/ml, corresponding to c roughly between 10^{-2} and 10^{-1} [51,52]. We carry out the simulations using LAMMPS [53], and thermalize the system to an average temperature $k_BT = 1.0$ through a Langevin thermostat [54]. A high monomer friction is imposed in order to simulate Brownian dynamics. To simulate filament annealing, each time two reactive sites come into contact a finite-extensible nonlinear elastic bond is created between them provided that the angle θ between prospective bonded triplets is larger than $\theta_{\text{min}} = 160°$ to prevent excessive accumulation of bending energies upon binding. Each monomer can form at most two bonds, so that when polymers are formed, only their ends act as reactive sites. See also the Supplemental Material.

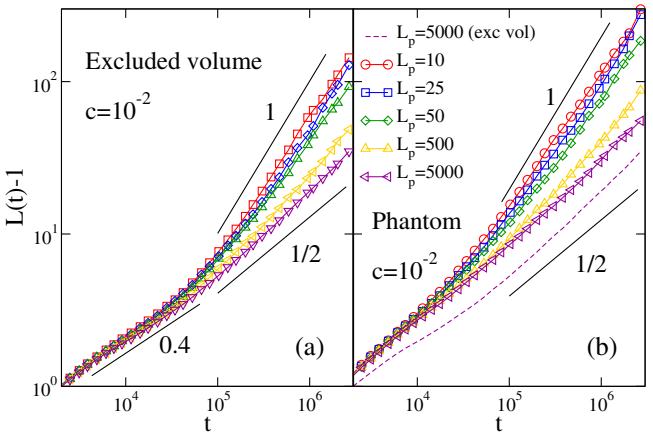

FIG. 3. Mean contour length as a function of time for excluded volume and phantom filaments with different persistence lengths L_p and concentration $c = 10^{-2}$. (a) Excluded volume. (b) Phantom. Dashed line: $L_p = 5000$ with excluded volume interactions [same as in panel (a), shown for comparison]. For both systems [(a) and (b)], the long-time behavior of $L(t)$ follows our predictions for the rigid rods (slope 1/2) and fluctuations-driven (slope 1) regimes, depending on L_p.

To assess the validity of our filament annealing dynamics dominated by diffusion and bending fluctuations, we monitor the mean filament contour length $L(t)$ and compare it to our scaling predictions. We start from a monomer solution, implying $L(0) = 1$, and thus monitor $L(t) - 1$. In Fig. 3(a) we show $L(t)$ for systems of polymers with monomer concentration $c = 10^{-2}$ and $10 \leq L_p \leq 5 \times 10^3$ (solid lines). At short times, namely for $1 \lesssim L - 1 \lesssim 3$, we observe a transient regime of sublinear growth $L(t) \propto t^\beta$ with $\beta \simeq 0.4$. We attribute this behavior to slower filament relaxation following binding in the presence of excluded volume interactions (Supplemental Material). After this transient, growth obeys a power law $L(t) \propto t^\beta$ where β

strongly depends on L_p. For large L_p, we observe $\beta = 1/2$, as predicted for rigid rods. As L_p is decreased, this exponent increases and approaches 1 (linear growth) as expected for the fluctuations-dominated regime.

As filaments elongate, many-body excluded volume interactions become more important and hinder diffusion [29]. This may drastically slow down the motion of the reactive sites, and could conceivably contribute to the observed crossover from sublinear ($\propto t^{1/2}$) to linear growth in Fig. 3(a). To prove that this crossover is instead due to the switching between a rigid rod regime and a fluctuations-dominated one, we simulate a system of "phantom" polymers [Fig. 3(b)]. There, the excluded volume interactions between nonbonded neighbors are removed so that distinct filaments can freely cross each other. The crossover from sublinear to linear growth is preserved in this system, implying that it is not caused by steric effects. There are, however, two differences with Fig. 3(a). First, at very early times L increases approximately as $t^{1/2}$ instead of $t^{0.4}$, suggesting that the transient regime discussed above may be caused by excluded volume effects. Secondly, the phantom polymers display a faster growth (1.5 to 2 times faster for $c = 10^{-2}$) both in the sublinear and in the linear regime [see dashed line in Fig. 3(b). To explain this second effect, one could speculate that excluded volume interactions slow down the movement of reactive sites and thus reduce the prefactor in the $x(t) \propto t^{3/8}$ relation. We show, however, that this is not the case by directly monitoring the mean-squared displacement of the end monomers of filaments that do not undergo annealing (Supplemental Material). Additionally, we also show that this effect is not due to significant differences in the filament length distribution for phantom and excluded volume filaments (Supplemental Material). This analysis also reveals that filaments that are either much shorter or much longer than L are rare, justifying *a posteriori* our scaling assumption of a single typical length governing the annealing kinetics. We instead attribute the slower assembly in nonphantom systems to the inaccessibility of some potential reaction partners due to steric hindrance [5,55].

Finally, to confirm that the main assembly mechanism switches from center-of-mass diffusion to bending fluctuations as filaments lengthen, we plot $(L-1)/L^*$ against t/t^*, where L^* and t^* are respectively the crossover length and time between the two regimes. Our model predicts that the data should collapse onto the same master curve, with the crossover taking place at $t/t^* \approx 1$, $(L-1)/L^* \approx 1$. We show that this is indeed the case in Fig. 4, although the collapse fails for filaments smaller than a dimer ($L \lesssim 2$), where the reaction rate is $K \approx b^3/\tau$ as expected for single monomers [56]. The collapse there is further distorted by dimerization events occurring within the first simulation time step in the denser regimes ($c \gtrsim 10^{-2}$). Following this initial regime (shaded area in Fig. 4), the data collapse on a master curve that displays a crossover between two

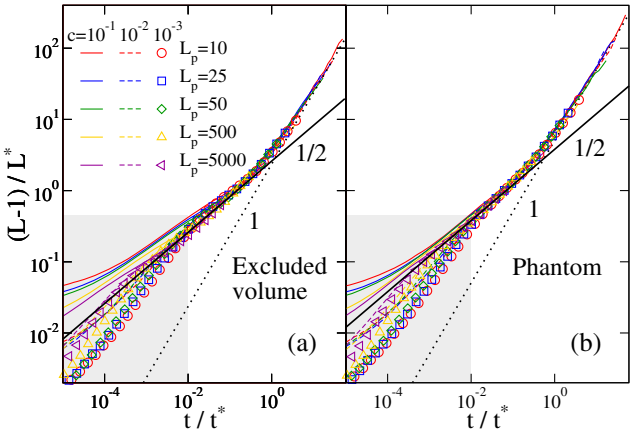

FIG. 4. Rescaled mean contour length as a function of time for excluded volume and phantom filaments with different persistence lengths L_p and concentrations $c = 10^{-3}$, 10^{-2}, and 10^{-1}. Here, $L^* = b(L_p/b)^{1/3}$ and $t^* = \tau(cb^3)^{-1}(L_p/b)^{2/3}$. (a) Excluded volume. (b) Phantom. For both systems [(a) and (b)], the data collapse on a single master curve, in agreement with the theoretical scaling regimes. The density-dependent behavior at small t (shaded area) is due to the rapid formation of a small number of bonds between nearby monomers at the very beginning of the simulation.

power-law regimes, confirming our theoretical predictions for both excluded volume and phantom systems. Indeed, we observe a regime with slope $1/2$ (rigid rod regime, dotted line), followed by a rather broad crossover to a linear one (fluctuations-driven regime, solid line). As an additional confirmation of the existence of this crossover, we also measure K directly from the reaction of same-length filaments, finding a good agreement with the scaling prediction (Supplemental Material). While we do not observe the Gaussian regime in our simulations, we recall that our theory predicts its onset only in very long filaments $L \gg L^{**} \propto L_p^{5/3}$. We thus estimate $L^{**} \approx 46$ for our smallest values of L_p, which may put this regime out of reach of our current simulations once geometrical prefactors are taken into account.

Overall, the fluctuations-driven regime predicted in this work allows for much faster growth of annealing semiflexible filaments compared to rigid rods. This mechanism is likely relevant in the cell cytoskeleton. In vimentin intermediate filaments with $L_p \simeq 1$ μm and $b \simeq 50$ nm [57,58], we expect our regime to dominate assembly for filament lengths comprised between $L^* \simeq 140$ nm and $L^{**} \simeq 7.4$ μm. This is consistent with the typical lengths between 200 nm and 10 μm observed in cells [59,60]. Estimating the resulting speedup in assembly as the ratio $K_{\text{semiflex}}/K_{\text{rigid}} \approx (L/b)(L_p/b)^{-1/3}$, where $K_{\text{rigid}} \approx k_B T b^2/\zeta L$ and K_{semiflex} is given by Eq. (4) yields a 40-fold speedup for a 5 μm vimentin filament. Actin filaments, which display significant end-to-end annealing under some conditions [18,19], may be similarly affected.

There, $L_p \simeq 18$ μm and $b \simeq 5.5$ nm [8] and so $L^* \simeq 82$ nm and $L^{**} \simeq 4.0$ mm, whereas the *in vivo* filament lengths are comprised between 100 nm and a few microns [61]. For a 5 μm actin filament, we estimate a speedup ratio of 60. Our analysis shows that transverse fluctuations dominate the assembly up to values of L^{**} much longer than the filament persistence length. This implies that the long-length Gaussian regime should very rarely, if ever, be observed. Our findings moreover shed new light on experimental observations of rigid-rod-like assembly kinetics ($K \propto L^{-1}$) in concentrated actin [19] and vimentin [55] undergoing annealing *in vitro*. These observations indicate that other phenomena such as lateral interactions (e.g., bundling [3–6]), may play a role in these experiments and effectively increase the rigidity of the filaments.

Our numerical simulations reveal that our mechanism does not give rise to widespread filament alignment, and that it is surprisingly robust to molecular crowding and excluded volume interactions. One could indeed naively expect excluded volume effects to significantly slow down network assembly when L becomes comparable with the mesh size $\xi \approx (cb)^{-1/2}$, as would be the case for diffusion in a suspension of rigid rods [29]. For a filament volume fraction $c = 10^{-2}$ ($c = 10^{-1}$), this would lead to significant excluded volume effects for filaments comprising more than ≈10 (3) monomers. By contrast, our theory accurately describes the simulated assembly dynamics well beyond these thresholds. This suggests that small-scale end fluctuations remain unhindered by neighboring filaments even in situations where the filament center-of-mass diffusion is largely inhibited, allowing the filaments to keep on annealing. These unhindered fluctuations are evidenced by the preservation of the $x(t) \propto t^{3/8}$ scaling for the filament end displacement even in the presence of excluded volume interactions [30] (Supplemental Material). This implies that filament assembly continues unabated into the $L > \xi$ "entangled network" regime of the semiflexible filament solution, where its short-term elastic modulus and its viscoelastic relaxation time both quickly increase with increasing filament length [62]. In cells, typical values of ξ range roughly between 100 and 500 nm [51,52]. This corresponds to reduced concentrations c between 10^{-2} and 0.25 for vimentin ($b \simeq 50$ nm). This is enough to strongly suppress the filaments' center-of-mass diffusion but not our fluctuations-driven mechanism, implying even larger speedup ratios than estimated above. The robustness of our assembly mechanism at high concentrations also justifies *a posteriori* neglecting hydrodynamic interactions, as these will be partially screened in concentrated systems [29]. Moreover, even in the dilute regime these interactions only lead to a logarithmic correction to the $x(t) \propto t^{3/8}$ scaling [34,38] and we thus do not expect them to significantly alter our predictions. Finally, in our simulations we have considered irreversible bonds and a finite monomer supply. However, knowledge of the annealing rate allows one in principle to describe the assembly kinetics also in the presence of severing [63] (if the severing mechanism is known) or equilibrium fragmentation [55]. Moreover, our assembly mechanism is robust with respect to the replenishment of monomers, which can be a relevant process in living cells (Supplemental Material).

Our estimates thus suggest that the mechanism described here may be crucial in allowing the cell to quickly assemble cytoskeletal structures in response to external stimuli. Beyond questions of timescales, these considerations may shift the balance between filament growth and, e.g., bundling or the buildup of entanglements during nonequilibrium cytoskeletal self-assembly. Indeed, It has been shown both in actin [5,64] and intermediate filaments [3,6] that differences in filament growth kinetics can lead to networks with markedly different mesh size, bundle density and diameter, and mechanical properties. Thus, the mechanism of growth kinetics is likely to have a profound impact on dictating the very structure and mechanics of cytoskeletal networks.

The authors thank Cécile Leduc and Duc-Quang Tran for invaluable help with understanding the experimental behavior of intermediate filaments, and Raphael Voituriez, Nicolas Levernier, and Alexander Grosberg for fruitful discussion on the theoretical model. V. S. also thanks Davide Michieletto, Maria Panoukidou, and Lorenzo Rovigatti for very helpful suggestions on the simulation model. M. L. was supported by Marie Curie Integration Grant No. PCIG12-GA-2012-334053, "Investissements d'Avenir" LabEx PALM (ANR-10-LABX- 0039-PALM), ANR Grants No. ANR-15-CE13-0004-03, No. ANR-21-CE11-0004-02 and No. ANR-22-CE30-0024, as well as ERC Starting Grant No. 677532. M. L.'s group belongs to the CNRS consortium AQV. Part of this work was performed using HPC resources from GENCI–IDRIS (Grants No. 2020-A0090712066 and No. 2021-A0110712066).

[1] M. T. Abreu-Blanco, J. J. Watts, J. M. Verboon, and S. M. Parkhurst, Cytoskeleton responses in wound repair, Cell Mol. Life Sci. **69**, 2469 (2012).

[2] A. Vivante, I. Shoval, and Y. Garini, The dynamics of lamin a during the cell cycle, Front. Mol. Biosci. **8**, 705595 (2021).

[3] J. Kayser, H. Grabmayr, M. Harasim, H. Herrmann, and A. R. Bausch, Assembly kinetics determine the structure of keratin networks, Soft Matter **8**, 8873 (2012).

[4] T. T. Falzone, P. W. Oakes, J. Sees, D. R. Kovar, and M. L. Gardel, Actin assembly factors regulate the gelation kinetics and architecture of F-actin networks, Biophys. J. **104**, 1709 (2013).

[5] G. Foffano, N. Levernier, and M. Lenz, The dynamics of filament assembly define cytoskeletal network morphology, Nat. Commun. **7**, 13827 (2016).

[6] A. V. Schepers, C. Lorenz, P. Nietmann, A. Janshoff, S. Klumpp, and S. Köster, Multiscale mechanics and temporal evolution of vimentin intermediate filament networks, Proc. Natl. Acad. Sci. U.S.A. **118**, e2102026118 (2021).
[7] L. Schween, N. Mücke, S. Portet, W. H. Goldmann, H. Herrmann, and B. Fabry, Dual-wavelength stopped-flow analysis of the lateral and longitudinal assembly kinetics of vimentin, Biophys. J. **121**, 3850 (2022).
[8] J. Howard, *Mechanics of Motor Proteins and the Cytoskeleton* (Sinauer Associates, inc., Sunderland, 2001).
[9] R. Sanghvi-Shah and G. F. Weber, Intermediate filaments at the junction of mechanotransduction, migration, and development, Front. Cell Dev. Biol. **5**, 81 (2017).
[10] G. Çolakoğlu and A. Brown, Intermediate filaments exchange subunits along their length and elongate by end-to-end annealing, J. Cell Biol. **185**, 769 (2009).
[11] S. Winheim, A. R. Hieb, M. Silbermann, E.-M. Surmann, T. Wedig, H. Herrmann, J. Langowski, and N. Mücke, Deconstructing the late phase of vimentin assembly by total internal reflection fluorescence microscopy (TIRFM), PLoS One **6**, e19202 (2011).
[12] I. Martin, A. Leitner, P. Walther, H. Herrmann, and O. Marti, Model-based analysis of keratin intermediate filament assembly, J. Phys. D **48**, 375401 (2015).
[13] H. Herrmann and U. Aebi, Intermediate filaments: Structure and assembly, Cold Spring Harbor Perspect. Biol. **8**, a018242 (2016).
[14] C. G. Lopez, O. Saldanha, K. Huber, and S. Köster, Lateral association and elongation of vimentin intermediate filament proteins: A time-resolved light-scattering study, Proc. Natl. Acad. Sci. U.S.A. **113**, 11152 (2016).
[15] M. Cates and S. Candau, Statics and dynamics of worm-like surfactant micelles, J. Phys. Condens. Matter **2**, 6869 (1990).
[16] L. Heinen and A. Walther, Programmable dynamic steady states in ATP-driven nonequilibrium DNA systems, Sci. Adv. **5**, eaaw0590 (2019).
[17] P. J. Flory, Fundamental principles of condensation polymerization, Chem. Rev. **39**, 137 (1946).
[18] D. Sept, J. Xu, T. D. Pollard, and J. A. McCammon, Annealing accounts for the length of actin filaments formed by spontaneous polymerization, Biophys. J. **77**, 2911 (1999).
[19] E. Andrianantoandro, L. Blanchoin, D. Sept, J. A. McCammon, and T. D. Pollard, Kinetic mechanism of end-to-end annealing of actin filaments, J. Mol. Biol. **312**, 721 (2001).
[20] S. W. Rothwell, W. A. Grasser, and D. B. Murphy, End-to-end annealing of microtubules *in vitro*, J. Cell Biol. **102**, 619 (1986).
[21] O. G. Berg and P. H. von Hippel, Diffusion-controlled macromolecular interactions, Annu. Rev. Biophys. Biophys. Chem. **14**, 131 (1985).
[22] G. Wilemski and M. Fixman, Diffusion-controlled intrachain reactions of polymers. I theory, J. Chem. Phys. **60**, 866 (1974).
[23] G. Wilemski and M. Fixman, Diffusion-controlled intrachain reactions of polymers. II results for a pair of terminal reactive groups, J. Chem. Phys. **60**, 878 (1974).
[24] S. Sunagawa and M. Doi, Theory of diffusion-controlled intrachain reactions of polymers, Polym. J. **7**, 604 (1975).
[25] M. Doi, Diffusion-controlled reaction of polymers, Chem. Phys. **9**, 455 (1975).
[26] P. De Gennes, Kinetics of diffusion-controlled processes in dense polymer systems. I. Nonentangled regimes, J. Chem. Phys. **76**, 3316 (1982).
[27] P. De Gennes, Kinetics of diffusion-controlled processes in dense polymer systems. II. Effects of entanglements, J. Chem. Phys. **76**, 3322 (1982).
[28] A. Y. Grosberg, P. G. Khalatur, and A. R. Khokhlov, Polymeric coils with excluded volume in dilute solution: The invalidity of the model of impenetrable spheres and the influence of excluded volume on the rates of diffusion-controlled intermacromolecular reactions, Makromol. Chem., Rapid Commun. **3**, 709 (1982).
[29] M. Doi and S. F. Edwards, *The Theory of Polymer Dynamics* (Oxford University Press, New York, 1986).
[30] P. Lang and E. Frey, Disentangling entanglements in biopolymer solutions, Nat. Commun. **9**, 494 (2018).
[31] P. G. J. Van Dongen and M. H. Ernst, Dynamic scaling in the kinetics of clustering, Phys. Rev. Lett. **54**, 1396 (1985).
[32] P. Van Dongen and M. Ernst, Scaling solutions of Smoluchowski's coagulation equation, J. Stat. Phys. **50**, 295 (1988).
[33] P. Meakin and M. H. Ernst, Scaling in aggregation with breakup simulations and mean-field theory, Phys. Rev. Lett. **60**, 2503 (1988).
[34] R. Granek, From semi-flexible polymers to membranes: Anomalous diffusion and reptation, J. Phys. II **7**, 1761 (1997).
[35] E. Farge and A. C. Maggs, Dynamic scattering from semiflexible polymers, Macromolecules **26**, 5041 (1993).
[36] L. Le Goff, O. Hallatschek, E. Frey, and F. Amblard, Tracer studies on F-actin fluctuations, Phys. Rev. Lett. **89**, 258101 (2002).
[37] A. Huang, A. Bhattacharya, and K. Binder, Conformations, transverse fluctuations, and crossover dynamics of a semiflexible chain in two dimensions, J. Chem. Phys. **140**, 214902 (2014).
[38] A. Nikoubashman, A. Milchev, and K. Binder, Dynamics of single semiflexible polymers in dilute solution, J. Chem. Phys. **145**, 234903 (2016).
[39] O. G. Berg, Diffusion-controlled protein–DNA association: Influence of segemental diffusion of the DNA, Biopolymers **23**, 1869 (1984).
[40] T. Guérin, M. Dolgushev, O. Bénichou, R. Voituriez, and A. Blumen, Cyclization kinetics of Gaussian semiflexible polymer chains, Phys. Rev. E **90**, 052601 (2014).
[41] See Supplemental Material at http://link.aps.org/supplemental/10.1103/PhysRevLett.131.228401, which includes Refs. [42–46], for (i) scaling argument to derive the time dependence of the typical length L in the fluctuations-driven regime, (ii) additional details on the simulation model, (iii) finite-size effects analysis, (iv) analysis of the filaments mean-squared displacement in the absence of assembly, (v) filament length distribution, (vi) direct measurement of the reaction rate, and (vii) robustness of the assembly mechanism with respect to monomer addition.

[42] J. D. Weeks, D. Chandler, and H. C. Andersen, Role of repulsive forces in determining the equilibrium structure of simple liquids, J. Chem. Phys. **54**, 5237 (1971).
[43] J. P. Wittmer, H. Meyer, J. Baschnagel, A. Johner, S. Obukhov, L. Mattioni, M. Müller, and A. N. Semenov, Long range bond-bond correlations in dense polymer solutions, Phys. Rev. Lett. **93**, 147801 (2004).
[44] H.-P. Hsu and K. Kremer, Static and dynamic properties of large polymer melts in equilibrium, J. Chem. Phys. **144**, 154907 (2016).
[45] R. Kirmse, S. Portet, N. Mücke, U. Aebi, H. Herrmann, and J. Langowski, A quantitative kinetic model for the *in vitro* assembly of intermediate filaments from tetrameric vimentin, J. Biol. Chem. **282**, 18563 (2007).
[46] S. Portet, N. Mücke, R. Kirmse, J. Langowski, M. Beil, and H. Herrmann, Vimentin intermediate filament formation: In vitro measurement and mathematical modeling of the filament length distribution during assembly, Langmuir **25**, 8817 (2009).
[47] P. Van Dongen and M. Ernst, Kinetics of reversible polymerization, J. Stat. Phys. **37**, 301 (1984).
[48] K. Kremer and G. S. Grest, Dynamics of entangled linear polymer melts: A molecular-dynamics simulation, J. Chem. Phys. **92**, 5057 (1990).
[49] C. Svaneborg and R. Everaers, Characteristic time and length scales in melts of Kremer–Grest bead–spring polymers with wormlike bending stiffness, Macromolecules **53**, 1917 (2020).
[50] M. Panoukidou, S. Weir, V. Sorichetti, Y. G. Fosado, M. Lenz, and D. Michieletto, Runaway transition in irreversible polymer condensation with cyclisation, arXiv:2210.14010.
[51] S. Sivaramakrishnan, J. V. DeGiulio, L. Lorand, R. D. Goldman, and K. M. Ridge, Micromechanical properties of keratin intermediate filament networks, Proc. Natl. Acad. Sci. U.S.A. **105**, 889 (2008).
[52] D. B. Bekker-Jensen, C. D. Kelstrup, T. S. Batth, S. C. Larsen, C. Haldrup, J. B. Bramsen, K. D. Sørensen, S. Høyer, T. F. Ørntoft, C. L. Andersen *et al.*, An optimized shotgun strategy for the rapid generation of comprehensive human proteomes, Cell Syst. **4**, 587 (2017).
[53] S. Plimpton, Fast parallel algorithms for short-range molecular dynamics, J. Comput. Phys. **117**, 1 (1995).
[54] T. Schneider and E. Stoll, Molecular-dynamics study of a three-dimensional one-component model for distortive phase transitions, Phys. Rev. B **17**, 1302 (1978).
[55] Q. D. Tran, V. Sorichetti, G. Pehau-Arnaudet, M. Lenz, and C. Leduc, Fragmentation and entanglement limit vimentin intermediate filament assembly, Phys. Rev. X **13**, 011014 (2023).
[56] F. Sciortino, C. De Michele, and J. F. Douglas, Growth of equilibrium polymers under non-equilibrium conditions, J. Phys. Condens. Matter **20**, 155101 (2008).
[57] N. Mücke, L. Kreplak, R. Kirmse, T. Wedig, H. Herrmann, U. Aebi, and J. Langowski, Assessing the flexibility of intermediate filaments by atomic force microscopy, J. Mol. Biol. **335**, 1241 (2004).
[58] F. N. Vicente, M. Lelek, J.-Y. Tinevez, Q. D. Tran, G. Pehau-Arnaudet, C. Zimmer, S. Etienne-Manneville, G. Giannone, and C. Leduc, Molecular organization and mechanics of single vimentin filaments revealed by super-resolution imaging, Sci. Adv. **8**, eabm2696 (2022).
[59] A. Robert, C. Hookway, and V. I. Gelfand, Intermediate filament dynamics: What we can see now and why it matters, BioEssays **38**, 232 (2016).
[60] E. Terriac, G. Coceano, Z. Mavajian, T. A. Hageman, A. F. Christ, I. Testa, F. Lautenschläger, and A. K. Gad, Vimentin levels and serine 71 phosphorylation in the control of cell-matrix adhesions, migration speed, and shape of transformed human fibroblasts, Cells **6**, 2 (2017).
[61] K. Kasza, C. Broedersz, G. Koenderink, Y. Lin, W. Messner, E. Millman, F. Nakamura, T. Stossel, F. MacKintosh, and D. Weitz, Actin filament length tunes elasticity of flexibly cross-linked actin networks, Biophys. J. **99**, 1091 (2010).
[62] C. P. Broedersz and F. C. MacKintosh, Modeling semi-flexible polymer networks, Rev. Mod. Phys. **86**, 995 (2014).
[63] C. Hookway, L. Ding, M. W. Davidson, J. Z. Rappoport, G. Danuser, and V. I. Gelfand, Microtubule-dependent transport and dynamics of vimentin intermediate filaments, Mol. Biol. Cell **26**, 1675 (2015).
[64] T. T. Falzone, M. Lenz, D. R. Kovar, and M. L. Gardel, Assembly kinetics determine the architecture of α-actinin crosslinked F-actin networks, Nat. Commun. **3**, 861 (2012).